nature communications

Article

https://doi.org/10.1038/s41467-024-50973-y

Neuro-intestinal acetylcholine signalling regulates the mitochondrial stress response in *Caenorhabditis elegans*

Received: 20 March 2024

Accepted: 25 July 2024

Published online: 03 August 2024

Check for updates

Rebecca Cornell[1], Wei Cao[1], Bernie Harradine[1], Rasoul Godini[1], Ava Handley[1] & Roger Pocock[1]

Neurons coordinate inter-tissue protein homeostasis to systemically manage cytotoxic stress. In response to neuronal mitochondrial stress, specific neuronal signals coordinate the systemic mitochondrial unfolded protein response (UPR^{mt}) to promote organismal survival. Yet, whether chemical neurotransmitters are sufficient to control the UPR^{mt} in physiological conditions is not well understood. Here, we show that gamma-aminobutyric acid (GABA) inhibits, and acetylcholine (ACh) promotes the UPR^{mt} in the *Caenorhabditis elegans* intestine. GABA controls the UPR^{mt} by regulating extrasynaptic ACh release through metabotropic GABA$_B$ receptors GBB-1/2. We find that elevated ACh levels in animals that are GABA-deficient or lack ACh-degradative enzymes induce the UPR^{mt} through ACR-11, an intestinal nicotinic α7 receptor. This neuro-intestinal circuit is critical for non-autonomously regulating organismal survival of oxidative stress. These findings establish chemical neurotransmission as a crucial regulatory layer for nervous system control of systemic protein homeostasis and stress responses.

Maintaining systemic mitochondrial function is crucial for organismal health and survival. Mitochondrial stress responses are essential molecular mechanisms that maintain metabolic homeostasis. Local stress responses can be communicated to distal tissues to systemically combat challenges, and thereby increase the chance of organismal survival. The nervous system is critical for coordinating stress responses across multiple tissues. Previous studies have revealed multiple neuronal signals that coordinate the systemic mitochondrial unfolded protein response (UPR^{mt}) when the nervous system is exposed to mitochondrial stress encountered in disease states[1–7]. In unstressed conditions, optimizing mitochondrial function in response to metabolic and physiological fluctuations is a continual process. However, whether the nervous system tonically regulates the UPR^{mt} in unstressed, physiological conditions is unclear. In this study, we aimed to better understand how the nervous system maintains systemic mitochondrial function and health.

Results

GABA Signalling Inhibits the Intestinal UPR^{mt}

Neurotransmission is a core communication mechanism of the nervous system. To identify neurotransmitters that mediate systemic mitochondrial health, we screened neurotransmitter synthesis and transport mutants for changes to intestinal expression of the *hsp-6p::gfp* reporter, a well-established readout for the UPR^{mt} [8–12]. We screened loss-of-function mutations affecting dopamine (*cat-2*), octopamine and tyramine (*tdc-1*), serotonin (*tph-1*), glutamate (*eat-4*), gamma-aminobutyric acid (GABA) (*unc-25*) and acetylcholine (ACh) (*cha-1*) signalling (Fig. 1a, b)[13–18]. We found that loss of UNC-25/GAD, a glutamic acid decarboxylase required for GABA synthesis (Fig. 1c), induced intestinal *hsp-6p::gfp* expression (Fig. 1a, b). UNC-25 is expressed in 26 GABAergic neurons: 19 D-type motor neurons, 4 RME motor neurons, and 3 other neurons (AVL, DVB and RIS) (Fig. 1d)[17]. Resupplying *unc-25* cDNA to all GABA expressing neurons using the *unc-25* promoter rescued intestinal *hsp-6p::gfp* expression levels in

[1]Development and Stem Cells Program, Monash Biomedicine Discovery Institute and Department of Anatomy and Developmental Biology, Monash University, Melbourne, VIC 3800, Australia. e-mail: roger.pocock@monash.edu

https://doi.org/10.1038/s41467-024-50973-y

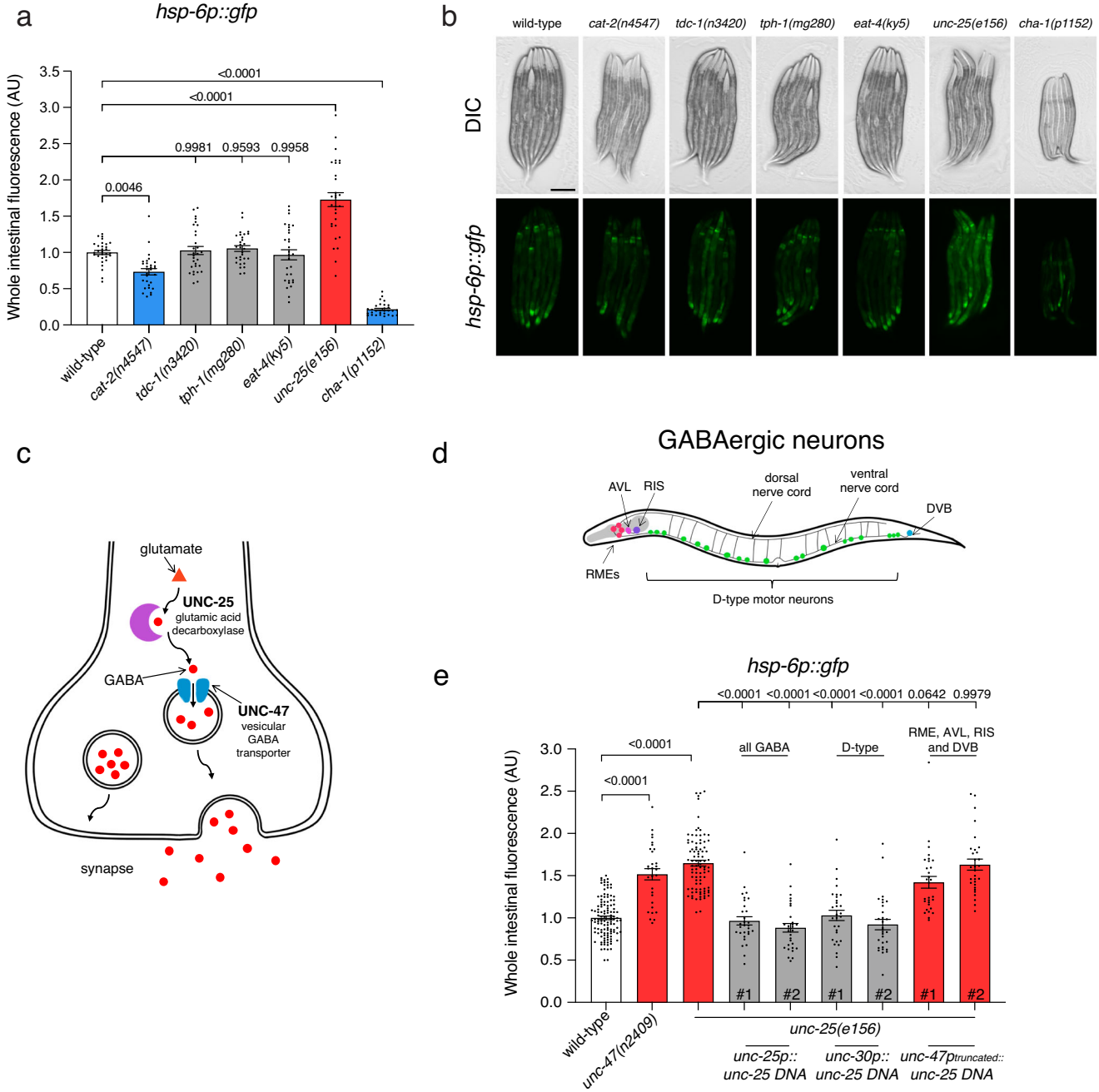

Fig. 1 | Gamma-aminobutyric acid (GABA) non-cell-autonomously inhibits the mitochondrial unfolded protein response (UPR^{mt}). **a**, **b** Quantification (**a**) and DIC/fluorescent micrographs (**b**) of UPR^{mt} reporter (*hsp-6p::gfp*) expression in L4 larvae of wild-type and mutant animals affecting neurotransmitter synthesis and transport. **c** Schematic of GABA synthesis (UNC-25/GAD), transport (UNC-47/VGAT), and release. **d** Schematic of GABA expressing neurons in *C. elegans*. **e** Quantification of UPR^{mt} reporter (*hsp-6p::gfp*) expression in L4 larvae of wild-type, *unc-47(n2409)*, *unc-25(e156)*, *unc-25(e156); unc-25p::unc-25 DNA*, *unc-25(e156); unc-30p::unc-25 DNA* and *unc-25(e156); unc-47p$_{truncated}$::unc-25 DNA* animals. $n = 30$ animals. The hash symbol (#) refers to independent transgenic rescue lines. *P* values assessed by one-way analysis of variance (ANOVA) with Tukey's post hoc test. Error bars indicate SEM. Scale bar, 250 µm. Source data are provided as a Source Data file.

unc-25(−) animals (Fig. 1e), confirming a role for UNC-25 in non-autonomous regulation of the intestinal UPR^{mt}. Furthermore, induced *hsp-6p::gfp* expression in *unc-25(−)* mutant animals was rescued by *unc-25* cDNA expression under the D-type motor neuron *unc-30* promoter, but not under the truncated *unc-47* promoter that drives expression in the RMEs, AVL, RIS and DVB neurons (Fig. 1e)[19].

Animals lacking UNC-25 also showed increased intestinal expression of another mitochondrial stress marker; *hsp-60p::gfp* (Supplementary Fig. 1a, b). Similarly, *sod-3p::gfp* expression—a DAF-16/FOXO transcription factor regulated gene with roles in combatting oxidative stress in mitochondria—was also induced in *unc-25(−)* animals (Supplementary Fig. 1c, d), consistent with previously published data[20,21]. We found that UNC-25 loss did not affect *hsp-16.2p::gfp*, a reporter for cytosolic heat stress, suggesting that disrupted GABA signalling does not induce a general stress response (Supplementary Fig. 1e, f). UPR^{mt} induction is regulated by ATFS-1, a mitochondrial unfolded protein response transcription factor, and the chromatin remodelling proteins DVE-1 and UBL-5[10,22]. Using RNA-mediated interference (RNAi), we silenced *atfs-1*, *ubl-5* and *dve-1* in *unc-25(−)* animals and found that intestinal *hsp-6p::gfp* induction was suppressed (Supplementary Fig. 1g, h). Therefore, GABA signalling requires canonical transcriptional regulators to activate the intestinal UPR^{mt}.

To corroborate the role of GABA signalling in controlling the intestinal UPR^{mt}, we analysed other components of the GABA signalling pathway (Fig. 1c, e and Supplementary Fig. 1i–k). The vesicular GABA transporter UNC-47/VGAT is required for packaging GABA into presynaptic vesicles for synaptic release[23,24]. We found that loss of *unc-47* induces *hsp-6p::gfp* expression (Fig. 1e and Supplementary Fig. 1i). The UNC-30/Pitx2 transcription factor is a terminal selector of D-type motor neuron identity, where it directly promotes *unc-25* and *unc-47* expression (Supplementary Fig. 1j)[25,26]. We found that *unc-30* loss also induced *hsp-6p::gfp* expression and that expressing *unc-30* DNA under the D-type motor neuron specific *unc-30* promoter rescued this phenotype (Supplementary Fig. 1k). In contrast, expressing *unc-30* in the intestine using the *ges-1* promoter did not affect *hsp-6p::gfp* expression (Supplementary Fig. 1k). Taken together, these data reveal that GABA signalling specifically from the D-type motor neurons represses the UPR^{mt} in the *C. elegans* intestine.

We next sought to determine how GABA influences mitochondria in distal tissues. Several GABA related processes regulate life and health-span, which are concepts closely related to mitochondrial health[27,28]. In *C. elegans*, GABA signalling transmits longevity signals through DAF-16/FOXO[20]. An intermediate component in this pathway is the PLCβ homologue, EGL-8[29]. We found that loss of *egl-8* did not induce intestinal *hsp-6p::gfp* expression (Supplementary Fig. 2a, c), suggesting that GABA signalling regulates the intestinal UPR^{mt} and longevity through different mechanisms. We wondered if GABA was acting as a metabolite to influence mitochondrial health through the GABA shunt, where GABA is degraded to succinic semialdehyde (SSA) by GABA-transaminase (GTA-1) and then joins the TCA cycle[30]. However, loss of the *C. elegans* GABA transaminase, GTA-1, did not influence intestinal *hsp-6p::gfp* expression (Supplementary Fig. 2b, c).

Regulation of acetylcholine release by GABA$_B$ receptors controls the intestinal UPR^{mt}

We speculated that GABA signalling mediates the UPR^{mt} from the D-type motor neurons by signalling to downstream GABA receptors. We therefore screened available GABA receptor mutants for *hsp-6p::gfp* induction, focusing on those receptors previously implicated in life and health-span[21]. We found that loss of the inhibitory UNC-49 and excitatory EXP-1 ionotropic GABA$_A$ receptors did not influence the intestinal UPR^{mt} (Fig. 2a–c)[31,32]. However, loss of both components of the metabotropic GABA$_B$ receptor—GBB-1 and GBB-2—induced intestinal *hsp-6p::gfp* expression (Fig. 2a–c). Intestinal *hsp-6p::gfp* expression in the *gbb-2(−); gbb-1(−)* compound mutant was not significantly different to either single mutant, indicating that both components of the GABA$_B$ receptor are required in the same pathway to control the UPR^{mt} (Fig. 2a–c). Likewise, intestinal *hsp-6p::gfp* expression in the *unc-25(−); gbb-2(−); gbb-1(−)* triple mutant was not additive compared the *unc-25(−)* single mutant, showing that GABA synthesis and the metabotropic GABA receptors act within the same genetic pathway to control the systemic UPR^{mt} (Fig. 2d). Mutant strains containing the *unc-25(e156)* mutation, however, exhibited slightly stronger *hsp-6p::gfp* expression than *gbb-1(−)* and *gbb-2(−)* mutants, suggesting that GABA signalling may also have roles outside of metabotropic signalling in controlling systemic UPR^{mt} activation. Canonically, GBB-1 and GBB-2 act in concert to reduce neuronal excitability, however, previous studies found that GBB-1 can act independently to influence longevity through DAF-16/FOXO[20]. This is supported by our data, where *sod-3p::gfp* expression—a readout for DAF-16 activity—is regulated by GBB-1, and not GBB-2 (Supplementary Fig. 3). These data support a role for GABA in UPR^{mt} activation independent to its role in longevity. Single cell sequencing data shows that *gbb-1* and *gbb-2* are expressed primarily in neurons[33]. Therefore, we resupplied *gbb-1* cDNA under the pan-neuronal *rgef-1* promoter in *gbb-1(−)* animals and found that this rescued the increased intestinal *hsp-6p::gfp* levels (Fig. 2e), confirming that the GABA$_B$ receptor complex acts in neurons to influence intestinal UPR^{mt} activation.

Within the *C. elegans* ventral nerve cord, D-type GABAergic motor neurons synapse with body wall muscle and adjacent cholinergic neurons, which are the only motor neurons that express *gbb-1* and *gbb-2* (Fig. 3a)[34,35]. To determine whether the metabotropic receptor complex acts in cholinergic motor neurons to mediate the intestinal UPR^{mt}, we resupplied *gbb-1* cDNA specifically to cholinergic ventral nerve cord motor neurons using a 1882bp *acr-2(s)* promoter[36]. We found that *gbb-1* expression in these cholinergic motor neurons rescued the increased intestinal *hsp-6p::gfp* levels of *gbb-1(−)* animals (Fig. 2e), confirming that the GABA$_B$ receptor complex acts in cholinergic motor neurons to influence intestinal UPR^{mt} activation. As GABA is generally an inhibitory neurotransmitter, and ACh is the primary excitatory neurotransmitter, these neurons work in a negative feedback loop to regulate each other and the muscles they innervate[37]. When the inhibitory GABA signal is lost, cholinergic neurons are overactive, leading to increased ACh release[35]. We therefore speculated that GABA regulates the intestinal UPR^{mt} through downstream ACh signalling. Our initial screening data showed that loss of the choline acetyltransferase CHA-1/ChAT, which is required for ACh production, significantly reduced intestinal *hsp-6p::gfp* expression (Fig. 1a). Likewise, loss of the ACh vesicular transporter UNC-17/VAChT also reduced intestinal *hsp-6p::gfp* expression (Fig. 3b, c). Importantly, loss of *unc-17* rescued the increased *hsp-6::gfp* observed in *unc-25(−)* and *gbb-1(−)* animals (Fig. 3b, c and Supplementary Fig. 4). These data support the concept that ACh levels can influence the systemic UPR^{mt}, and that increased ACh release in animals lacking GABA signalling would increase the intestinal UPR^{mt}. To test this hypothesis, we examined animals lacking two acetylcholinesterases, ACE-1/2, which have an approximately two-fold increase in systemic ACh[38]. We found that, as with loss of GABA signalling, increased ACh in *ace-2(−); ace-1(−)* animals induced intestinal *hsp-6p::gfp* expression (Fig. 3d, e).

The intestinal ACR-11 nicotinic α7 receptor regulates mitochondrial health

We theorized that excess ACh acts directly on intestinal cells to induce the UPR^{mt}. Therefore, we used RNAi to knock down intestinally-expressed ACh receptors (ACR-6, ACR-7 and ACR-11) in the *ace-2(−); ace-1(−)* compound mutant, screening for inhibition of *hsp-6p::gfp* induction (Fig. 3f). This analysis revealed that only knockdown of the nicotinic α7 receptor (α7 nAChR) ACR-11, an ortholog of human CHRNA7, abrogated intestinal *hsp-6p::gfp* induction in *ace-2(−); ace-1(−)* animals (Fig. 3f). Importantly, ACR-11 knockdown also prevented *hsp-6p::gfp* induction in *unc-25(−)* animals (Fig. 3g). To corroborate our RNAi results, we used CRISPR/Cas9 to generate independent *acr-11* deletions in wild type and *ace-2(−); ace-1(−)* mutant animals (Fig. 4a). As *acr-11* and *ace-2* are tightly linked on chromosome I, the *acr-11* deletions were generated separately. Confirming our RNAi data, the *acr-11(rp192)* deletion prevented *hsp-6p::gfp* induction in *ace-2(−); ace-1(−)* animals (Fig. 4b). However, loss of *acr-11* alone was not sufficient to lower *hsp-6p::gfp* expression, as observed in *unc-17* mutant animals (Fig. 4b, c, e). We wondered whether other intestinal α7 nAChR may support optimal UPR^{mt} activation in conditions of physiological ACh levels. We therefore used CRISPR/Cas9 to generate *acr-6* and *acr-7* deletions (Fig. 4a) and measured *hsp-6p::gfp* levels in single, double and triple mutant combinations with *acr-11(rp191)* animals. We found that *hsp-6p::gfp* was only reduced when all three intestinally expressed α7 nAChR were deleted (Fig. 4c). This implies a small but significant role for ACR-6 and ACR-7 in UPR^{mt} activation under basal ACh conditions, with ACR-11 the main responder to elevated ACh.

To examine the expression pattern of *acr-11*, we generated transgenic animals expressing green fluorescent protein (GFP) under control of the 2024 bp *acr-11* promoter and detected expression in the intestine and pharynx, and not in neurons or body wall muscle (Supplementary Fig. 5). To determine whether ACR-11 is

https://doi.org/10.1038/s41467-024-50973-y

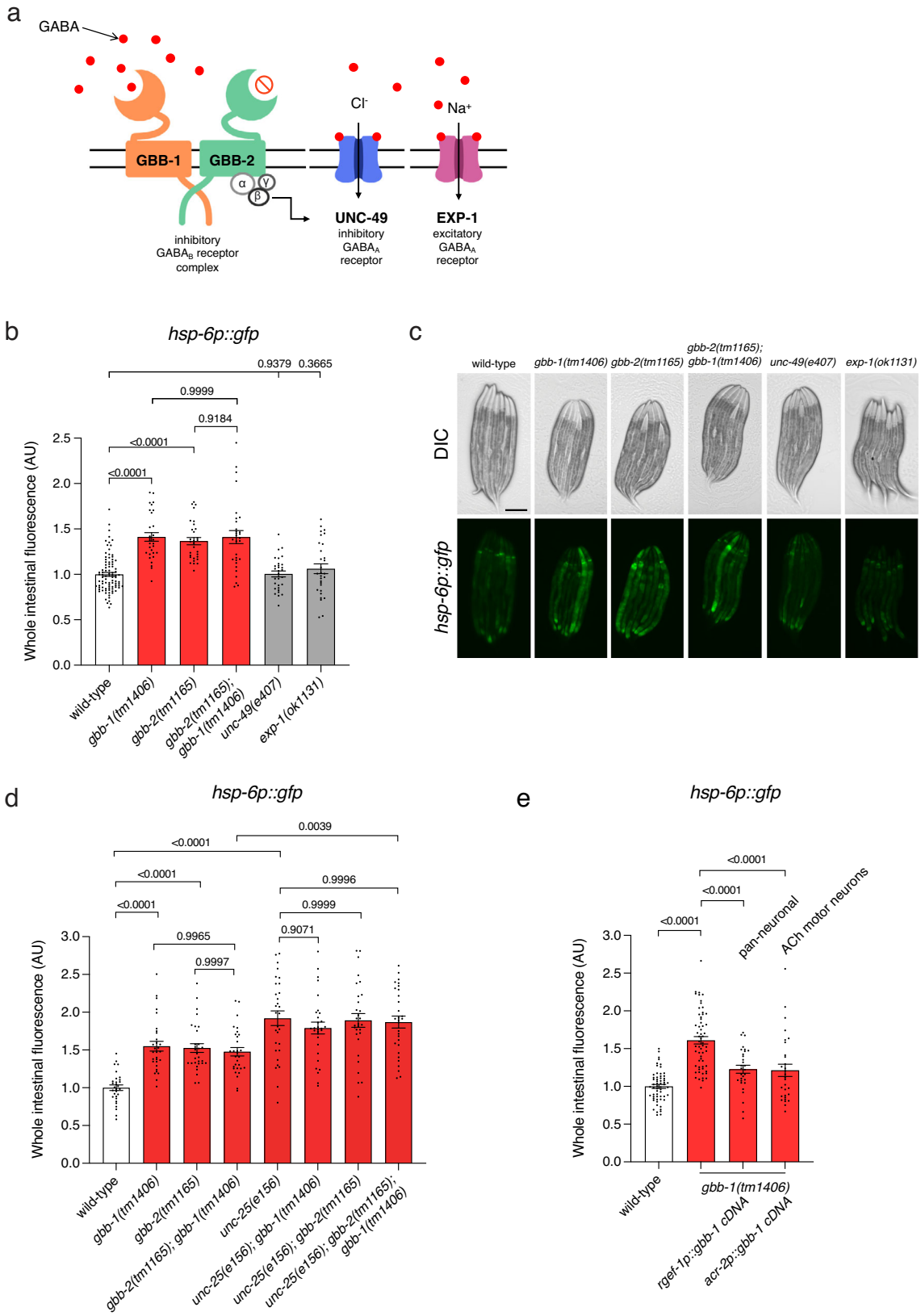

Fig. 2 | Metabotropic $GABA_B$ receptors coordinate non-cell-autonomous UPR^{mt}. **a** Schematic of ionotropic $GABA_A$ (UNC-49 (inhibitory) and EXP-1 (excitatory)) and metabotropic (GBB-1 and GBB-2) $GABA_B$ receptors in *C. elegans*. **b**, **c** Quantification (**b**) and DIC/fluorescent micrographs (**c**) of UPR^{mt} reporter (*hsp-6p::gfp*) expression in L4 larvae of wild-type, *gbb-1(tm1406)*, *gbb-2(tm1165)*, *gbb-2(tm1165); gbb-1(tm1406)*, *unc-49(e407)* and *exp-1(ok1131)* animals. **d** Quantification of UPR^{mt} reporter (*hsp-6p::gfp*) expression in L4 larvae of wild-type, *gbb-1(tm1406)*, *gbb-2(tm1165)*, *gbb-2(tm1165); gbb-1(tm1406)*, *unc-25(e156)*, *unc-25(e156); gbb-1(tm1406)*, *unc-25(e156); gbb-2(tm1165)*, and *unc-25(e156); gbb-2(tm1165); gbb-1(tm1406)* animals. **e** Quantification of UPR^{mt} reporter (*hsp-6p::gfp*) expression in L4 larvae of wild-type, *gbb-1(tm1406)*, *gbb-1(tm1406); rgef-1p::gbb-1 cDNA* and *gbb-1(tm1406); acr-2p(s)::gbb-1 cDNA* animals. $n = 30$ animals. *P* values assessed by one-way analysis of variance (ANOVA) with Tukey's post hoc test. Error bars indicate SEM. Scale bar, 250 μm. Source data are provided as a Source Data file.

https://doi.org/10.1038/s41467-024-50973-y

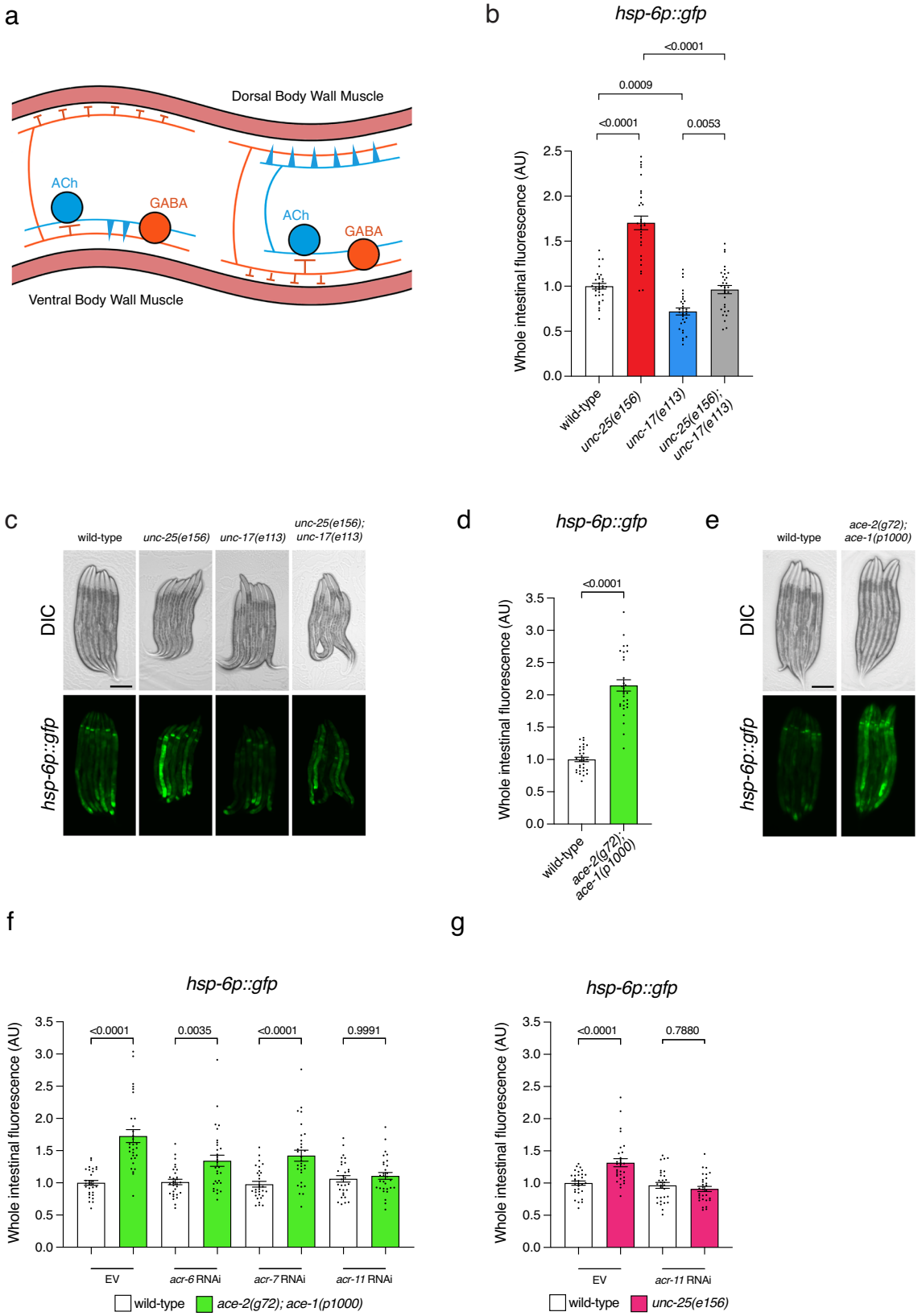

required in the intestine, we resupplied *acr-11* cDNA in the intestine (*ges-1* promoter) to the *ace-2(−) acr-11(−); ace-1(−)* triple mutant, which restored the *hsp-6p::gfp* expression levels to that of the *ace-2(−); ace-1(−)* double mutant (Fig. 4d, e). Furthermore, we found that *acr-11* overexpression in the intestine greatly induced *hsp-6p::gfp* expression in wild-type animals, and that this induction is rescued by preventing ACh release using an *unc-17* mutation (Fig. 4f, g). These data reveal that ACh acts through ACR-11 in the intestine to regulate the UPR^{mt}.

Calcium plays key roles in mitochondrial signalling, function and health, including in stress response activation[39,40]. As ACR-11 is an α7 nAChR, which are highly permeable to calcium ions[41], we investigated

Fig. 3 | Acetylcholine promotes non-cell-autonomous UPR^{mt} through the intestinal ACR-11/nicotinic α7 receptor. a Schematic of the *C. elegans* motor circuit. Orange = inhibitory GABAergic motor neurons; blue = excitatory cholinergic motor neurons; Pink = body wall muscle. **b**, **c** Quantification (**b**) and DIC/fluorescent micrographs (**c**) of UPR^{mt} reporter (*hsp-6p::gfp*) expression in L4 larvae of wild-type, *unc-25(e156), unc-17(e113),* and *unc-25(e156); unc-17(e113)* animals. **d**, **e** Quantification (**d**) and DIC/fluorescent micrographs (**e**) of UPR^{mt} reporter (*hsp-6p::gfp*) expression in L4 larvae of wild-type and *ace-2(g72); ace-1(p1000)* animals. **f** Quantification of UPR^{mt} reporter (*hsp-6p::gfp*) expression in L4 larvae of wild-type and *ace-2(g72); ace-1(p1000)* animals grown on empty vector (EV), *acr-6*, *acr-7* or *acr-11* RNAi from the mother's L4 stage. **g** Quantification of UPR^{mt} reporter (*hsp-6p::gfp*) expression in L4 larvae of wild-type and *unc-25(e156)* animals grown on empty vector (EV) or *acr-11* RNAi from the mother's L4 stage. $n = 30$ animals. *P* values assessed by one-way analysis of variance (ANOVA) Tukey's post hoc test (**b**, **f**, **g**) and two-way unpaired *t* test with Welch's correction (**d**). Error bars indicate SEM. Scale bars, 250 μm. Source data are provided as a Source Data file.

intracellular calcium storage using an intestine-specific fluorescence resonance energy transfer (FRET)-based calcium indicator[42,43] in animals with perturbed GABA and ACh signalling (Fig. 5a-b). We found that both *unc-25(−)* and *ace-2(−); ace-1(−)* animals had increased intracellular calcium levels (Fig. 5a, b). Furthermore, animals lacking ACR-11, either alone or when combined with the *ace-2(−); ace-1(−)* compound mutant, had wild-type calcium levels (Fig. 5a, b). These data mirror *hsp-6p::gfp* reporter levels in these mutants, supporting our hypothesis that ACR-11 responds to ACh release by increasing intracellular calcium levels in the intestine, which likely activates the UPR^{mt}.

UPR^{mt} activation can have a positive or negative effect on mitochondrial health[44]. An overactive stress response in the absence of stressors may prime mitochondria to manage subsequent stress exposure. Conversely, UPR^{mt} induction due to poor mitochondrial health may cause sensitivity to mitochondrial stressors. To assess whether perturbed GABA/ACh signalling influences mitochondrial stress resistance, we examined acute paraquat sensitivity. Paraquat exposure induces mitochondrial stress by disrupting complex I of the electron transport chain and increases superoxide levels[45]. We found that loss of GABA biosynthesis (*unc-25* mutant) or metabotropic GABA receptors (*gbb-1* and *gbb-2* mutants) were sensitive to paraquat (Fig. 5c and Supplementary Fig. 6a). Paraquat sensitivity was rescued in the *gbb-1(tm1406)* mutant by resupplying *gbb-1* cDNA in neurons (Fig. 5c). Further, we found that *ace-2(−); ace-1(−)* animals were sensitive to paraquat exposure (Fig. 5d). Thus, two conditions where ACh signalling is amplified cause sensitivity to a mitochondrial stressor. In contrast, *acr-11(−)* single and *ace-2(−) acr-11(−); ace-1(−)* triple mutant animals exhibited increased paraquat resistance (Fig. 5d). Neither *acr-6(−)* nor *acr-7(−)* caused changes to paraquat survival (Supplementary Fig. 6b), highlighting the specific importance of ACR-11. Furthermore, reduced ACh signalling in *unc-17(−)* animals conferred paraquat resistance, and was sufficient to rescue paraquat sensitivity induced by loss of *unc-25* (Fig. 5e). We found that intestinal *acr-11* cDNA overexpression severely impeded paraquat survival (Fig. 5f), mirroring the dramatic increase in *hsp-6p::gfp* expression observed when *acr-11* is overexpressed in the intestine. This sensitivity to paraquat was rescued by reducing ACh signalling via loss of *unc-17* (Fig. 5f). Therefore, increased UPR^{mt} activation via increased ACh signalling to ACR-11 is associated with mitochondrial damage and paraquat sensitivity, whilst decreased ACh signalling to ACR-11 is associated with increased mitochondrial fitness, leading to increased paraquat survival.

Another indicator of mitochondrial health is mitochondrial morphology. In general, more mitochondrial fusion indicates increased OXPHOS functionality, whereas more mitochondrial fragmentation indicates increased autophagy and/or biogenesis[46]. Based on our paraquat data, we hypothesized that *unc-25(−)* and *ace-2(−); ace-1(−)* animals would have more fragmented mitochondria, and that *acr-11(−)* single and *ace-2(−) acr-11(−); ace-1(−)* triple mutants would have increased mitochondrial fusion. Using a mitochondrial-targeted GFP reporter expressed in the intestine (*ges-1p::gfp^{mt}*)[47], we found that *unc-25(−)* and the *ace-2(−); ace-1(−)* animals had increased mitochondrial fragmentation in the intestine compared to wild type animals, as predicted (Supplementary Fig. 7a). This phenotype was intestine-specific, as we did not detect mitochondrial morphology changes in body wall muscle using a ubiquitously expressed reporter (*cox-4p::gfp^{mt}*) in *unc-25(−)* animals (Supplementary Fig. 7c, d)[48]. Unexpectedly, the *acr-11(−)* single mutant also displayed a fragmented mitochondria phenotype (Supplementary Fig. 7a). Further, the *ace-2(−) acr-11(−); ace-1(−)* triple mutant exhibited more mitochondrial fragmentation than the *acr-11(−)* single and *ace-2(−); ace-1(−)* double mutants (Supplementary Fig. 7a). These data imply that, in the context of mitochondrial morphology, ACh signalling and the ACR-11 receptor act in distinct pathways.

We wondered how similar mitochondrial fragmentation phenotypes observed in *unc-25(−), ace-2(−); ace-1(−)* and *acr-11(−)* animals could lead to opposing mitochondrial fitness in terms of paraquat resistance. We posited that, in a pathway separate from GABA/ACh signalling, ACR-11 may repress autophagy and thus mitochondrial turnover, perhaps as an energy conservation mechanism. This means that ACR-11 loss would induce fragmentation as mitochondria are excessively cleared from the system. Using an *mCherry::gfp::lgg-1* reporter to measure autophagy[49], we indeed found that the number of intestinal autophagosomes and autolysosomes in *acr-11(−)* L4 larvae is higher compared to control animals (Fig. 5g–i). This suggests that animals lacking ACR-11 exhibit elevated mitochondrial turn-over in unstressed conditions that conveys a survival advantage when exposed to oxidative stress.

Discussion

In summary, we discovered a neuro-intestinal circuit that regulates the UPR^{mt} and organismal survival. By screening animals lacking specific neurotransmitters, we found that balanced GABAergic and cholinergic signalling is essential for non-cell-autonomous UPR^{mt} regulation. We found that GABA released from ventral nerve cord motor neurons controls the UPR^{mt} through two metabotropic $GABA_B$ receptor subunits that are expressed on, and inhibit, cholinergic motor neurons. Appropriate control of ACh levels is critical for UPR^{mt} regulation, as animals lacking the ACh-degradative enzymes exhibit a two-fold induction of the UPR^{mt}. Further, we discovered that UPR^{mt} induction by increased systemic ACh is dependent on ACR-11, an α7 nAChR receptor acting in the intestine. Other intestinally expressed α7 nAChR receptors—ACR-6 and ACR-7—also play a minor role, in that all three receptors are required for mediating basal intestinal UPR^{mt} levels when systemic ACh is within a normal range. In addition to regulating the UPR^{mt}, elevated ACh induces mitochondrial fragmentation and reduces survival of oxidative stress. Interestingly, we found that the ACR-11 α7 nAChR receptor can act independently to ACh, with animals lacking ACR-11 exhibiting more intestinal mitochondrial fragmentation and autophagy irrespective of ACh levels. These distinctions likely provide animals lacking ACR-11 a survival advantage in oxidative stress conditions. In vertebrates, nicotinic α7 receptors can act in the liver (some functions of which are performed by the *C. elegans* intestine) to promote cell survival[50], suggesting that mechanisms we describe here are phylogenetically conserved.

Methods

C. elegans culture

All *C. elegans* strains were grown at 20 °C on NGM agar seeded with *Escherichia coli* OP50, unless otherwise stated. All mutant strains were backcrossed to N2 at least three times and maintained well fed for a

https://doi.org/10.1038/s41467-024-50973-y

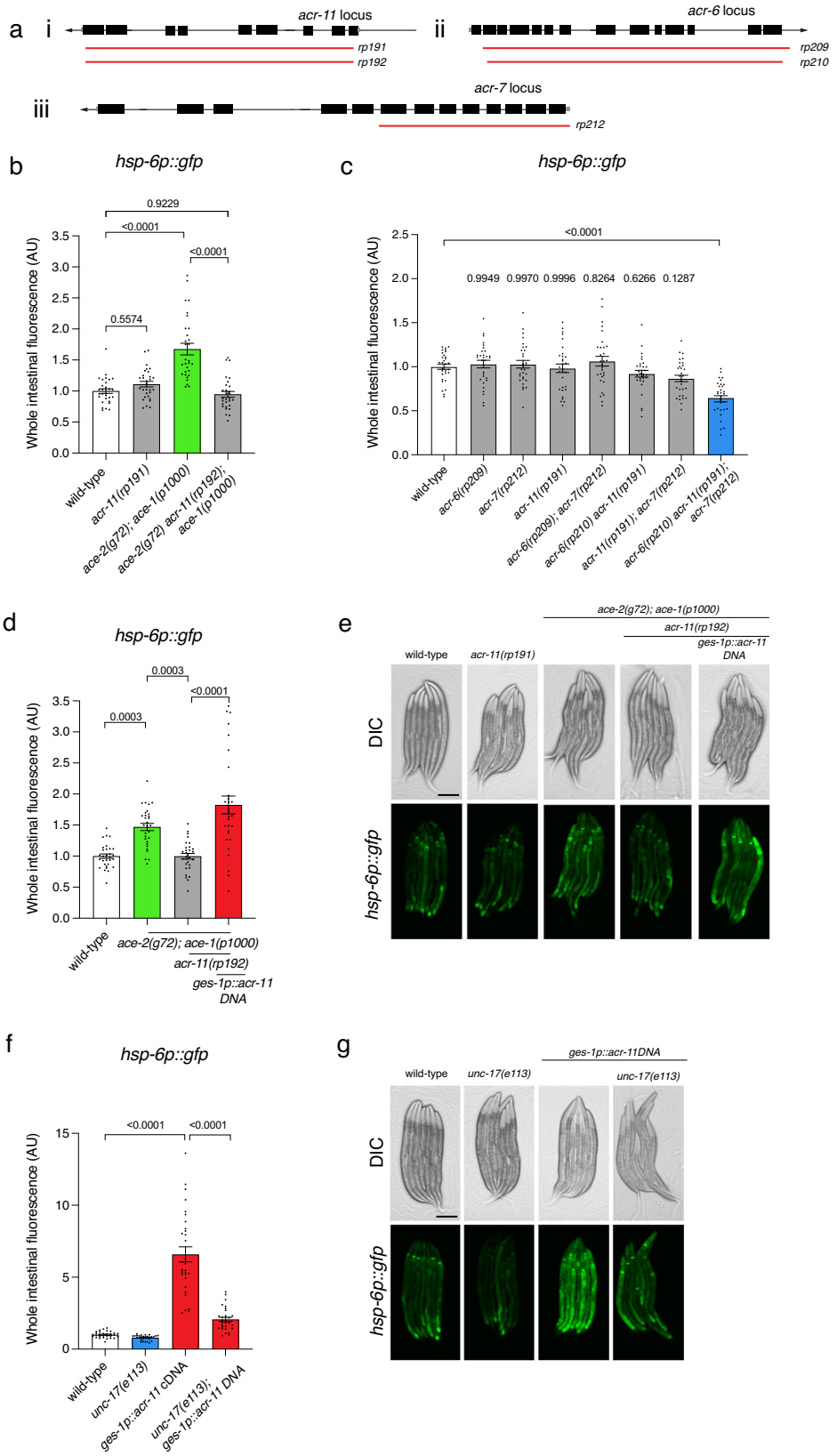

minimum of two generations prior to analysis. Strains used in this study are listed in Supplementary Table 1.

Fluorescence microscopy and quantification

Worms were anesthetised in 0.1 ng/ml levamisole on a 5% agarose pad. Images for analysis were taken using a Zeiss AXIO Imager M2 upright fluorescence microscope and ZEN 2.0 software at 20× objective, unless otherwise specified. ImageJ software was used to determine whole intestinal fluorescence by isolating the intestine area and measuring integrated density (IntDensity). The corrected cellular fluorescence was calculated as: CTCF = Intestinal Integrated Density−(area * background MeanGrey)

Fig. 4 | The ACR-11/nicotinic α7 receptor cell autonomously mediates the UPR^{mt}. **a** (i) Structure of the *acr-11* locus. *rp191* = 3038 bp deletion in wild-type animals; *rp192* = 3046 bp deletion in *ace-2(g72); ace-1(p1000)* animals. (ii) Structure of the *acr-6* locus. *rp209* = 3209 bp deletion in wild-type animals; *rp210* = 3158 bp deletion in *acr-11(rp191)* animals. (iii) Structure of the *acr-7* locus. *rp212* = 1556 bp deletion. Black boxes, coding regions; grey boxes, untranslated regions; red lines, CRISPR/Cas9-generated deletion alleles. **b** Quantification of UPR^{mt} reporter (*hsp-6p::gfp*) expression in L4 larvae of wild-type, *acr-11(rp191), ace-2(g72); ace-1(p1000)*, and *ace-2(g72) acr-11(rp192); ace-1(p1000)* animals. **c** Quantification of UPR^{mt} reporter (*hsp-6p::gfp*) expression in L4 larvae of wild-type, *acr-6(rp209), acr-7(rp212), acr-11(rp191), acr-6(rp209); acr-7(rp212), acr-6(rp210) acr-11(rp191), acr-11(rp191); acr-7(rp212)* and *acr-6(rp210) acr-11(rp191); acr-7(rp212)* animals. **d**, **e** Quantification (**d**) and DIC/fluorescent micrographs (**e**) of UPR^{mt} reporter (*hsp-6p::gfp*) expression in L4 larvae of wild-type, *ace-2(g72); ace-1(p1000), acr-11(rp191), ace-2(g72) acr-11(rp192); ace-1(p1000)* and *ace-2(g72) acr-11(rp192); ace-1(p1000); ges-1p::acr-11 DNA* animals. **f**, **g** Quantification (**f**) and DIC/fluorescent micrographs (**g**) of UPR^{mt} reporter (*hsp-6p::gfp*) expression in L4 larvae of wild-type, *unc-17(e113), ges-1p::acr-11 DNA* and *unc-17(e113); ges-1p::acr-11 cDNA* animals. *n* = 30 animals. *P* values assessed by one-way analysis of variance (ANOVA) with Tukey's post hoc test. Error bars indicate SEM. Scale bars, 250 μm. Source data are provided as a Source Data file.

RNA-mediated interference (RNAi) by feeding

HT115 bacteria containing control (L4440 plasmid) or experimental plasmids were cultured overnight in LB containing 50 μg/ml ampicillin and seeded uniformly over plates containing IPTG (Isopropyl β- d-1-thiogalactopyranoside). Plates were dried at 37 °C and brought to room temperature before worms were applied. For *atfs-1* and *ubl-5* RNAi experiments, five L4 hermaphrodites were picked to RNAi plates and the subsequent generation was scored at L4. For *dve-1* RNAi experiments, five L4 hermaphrodites were picked to NGM and allowed to grow for five days. Animals were then washed from the NGM plates using M9 and bleached for 4 min using a 1:1 ratio of bleach (White King Premium) and 5 M NaOH to extract eggs. Extracted eggs were washed three times in M9 and filtered through a 40 μm mesh before being applied to RNAi plates. Animals were grown to L4 and imaged as described above.

C. elegans expression constructs and transgenic strain generation

Reporter gene constructs were generated by PCR amplifying DNA elements and cloning into Fire vectors. Constructs were injected into young adult hermaphrodites using standard methods.

acr-11p::gfp reporter construct

A 2024 bp sequence upstream of the *acr-11* start codon was amplified from *C. elegans* genomic DNA with forward (GAAATGAAATAAGCTTGCGAAGAGAGCGAGGAGG) and reverse (CCAATCCCGGGGATCCTTCAAAAAAATGTGGCTAAG) primers from Sigma-Aldrich incorporating *HindIII-BamHI* restriction sites. The *HindIII-BamHI* digested promoter fragment was ligated into *HindIII-BamHI* digested pPD95.75 vector. The resultant *acr-11p::gfp* plasmid was injected at 50 ng/μl, with 50 ng/μl of *ttx-3p::mCherry* vector and 120 ng/μl bacterial DNA.

ges-1p::acr-11 rescue construct

The 1386 bp *acr-11* cDNA was amplified from a *C. elegans* cDNA library with forward (AGGACCCTTGGCTAGCATGATATTTAATCTAATTAATAG) and reverse (GATATCAATACCATGGTTAGGCAATAATATGAGG) primers from Sigma-Aldrich incorporating *NheI-NcoI* restriction sites. The *Pges-1p-sphk-1* vector was digested with *NheI-NcoI* and the *acr-11* cDNA was inserted using the In-Fusion HD Cloning Kit (Takara Bio) to replace the *sphk-1* sequence. The resultant *ges-1p::acr-11cDNA* plasmid was injected at 10 ng/μl, with 50 ng/μl of *ttx-3p::mCherry* vector and 120 ng/μl bacterial DNA into *acr-11* mutant animals for rescue, or wild-type for overexpression.

unc-25 rescue strains

The plasmids pHP03 [*unc-25p::unc25::unc-25 3′ UTR*], pNK06 [*unc-47p$_{truncated}$::unc-25::SL2::GFP::unc-54 3′ UTR*], pNK07 [*unc-30p::unc-25::SL2::GFP::unc-54 3′UTR*] were kindly provided by Haijun Tu. pNK06, was injected at 20 ng/μl[19]. pHP03 and pNK07 were injected at 1 ng/μl. All plasmids were injected with 50 ng/μl of *Pttx-3::mCherry* vector and 120 ng/μl bacterial DNA into *unc-25(e156); hsp-6::GFP* animals.

unc-30 rescue strains

pJL24 [*unc-30p::unc-30::SL2::GFP::unc-54 3′ UTR*], kindly provided by Haijun Tu, was injected at 1 ng/μl. RJP807 *ges-1p::unc-30 cDNA* was constructed by amplifying the *unc-30* cDNA from pJL24 with forward (AGGACCCTTGGCTAGCATGGATGACAATACGGCCACAC) and reverse (GATATCAATACCATGGCTAAAGTGGTCCACTGTACTGAC) primers incorporating *NheI-NcoI* restriction sites. RJP807 was injected at 10 ng/μl. All plasmids were injected with 50 ng/μl of *ttx-3p::mCherry* vector and 120 ng/μl bacterial DNA into *unc-30(e191); hsp-6::GFP* animals.

gbb-1 motor neuron rescue

The *acr-2p(s)::gbb-1* sequence was amplified by PCR from pBS77 (*Pacr-2-gbb-1 cDNA*) with forward (GCTCACCACCGACTGATTTTC) and reverse (TTGCGGTCATAAACTGAAACG) primers and injected at 5 ng/μl into *gbb-1(tm1406); hsp-6::GFP* animals with 50 ng/μl of *ttx-3p::mCherry* vector and 120 ng/μl bacterial DNA.

CRISPR-Cas9 genome editing

To generate *acr-11* deletion mutants, adult wild-type or *ace-2(p1000)I; ace-1(g72)X* hermaphrodites were microinjected with Cas9 protein and two crRNAs: 5′ crRNA (CCTGTGCGACGGAAGTGTTG), 3′ crRNA (CGAATCTCCAATCCGTTTGA) from IDT. *acr-11* deletions were identified by PCR and confirmed by Sanger sequencing. The *acr-11(rp191)* allele generated in wild-type animals is a 3038 bp deletion and the *acr-11(rp192)* allele generated in *ace-2(g72)I; ace-1(p1000)X* animals is a 3046 bp deletion. Both deletion alleles remove most of the *acr-11* gene (Fig. 4a(i)). Each allele was backcrossed to wild-type males prior to analysis.

To generate *acr-6* deletion mutants, adult wild-type or *acr-11(rp191)* mutant hermaphrodites were microinjected with Cas9 protein and two crRNAs: 5′ crRNA (GTATTGTTGAACTCACCAGA), 3′ crRNA (ATTCACGGATTGATAGCAAT) from IDT. *acr-6* deletions were identified by PCR and confirmed by Sanger sequencing. The *acr-6(rp209)* allele generated in wild-type animals is a 3209 bp deletion and the *acr-6(rp210)* allele generated in *acr-11(rp191)* animals is a 3158 bp deletion. Both deletion alleles remove most of the *acr-6* gene (Fig. 4a(ii)). Each allele was backcrossed twice to wild-type males prior to analysis.

To generate the *acr-7* deletion mutant, adult wild-type hermaphrodites were microinjected with Cas9 protein and two crRNAs: 5′ crRNA (ATTCACTCCTCATAGACGAG), 3′ crRNA (TTTTCACGTATTTACTACCAT) from IDT. The *acr-7* deletion was identified by PCR and confirmed by Sanger sequencing. The *acr-7(rp212)* allele is a 1556 bp deletion that removes the first 8 exons (Fig. 4a(iii)). The *acr-7(rp212)* allele was backcrossed twice to wild-type males prior to analysis.

Calcium imaging

Calcium levels were visualised using the calcium indicator d3cpv expressed in the intestine using the *nhx-2* intestine-limited promoter[43]. Worms were anesthetised with in 0.1 ng/ml levamisole diluted in M9 and mounted to 5% agarose pads. Images were taken using Leica

https://doi.org/10.1038/s41467-024-50973-y

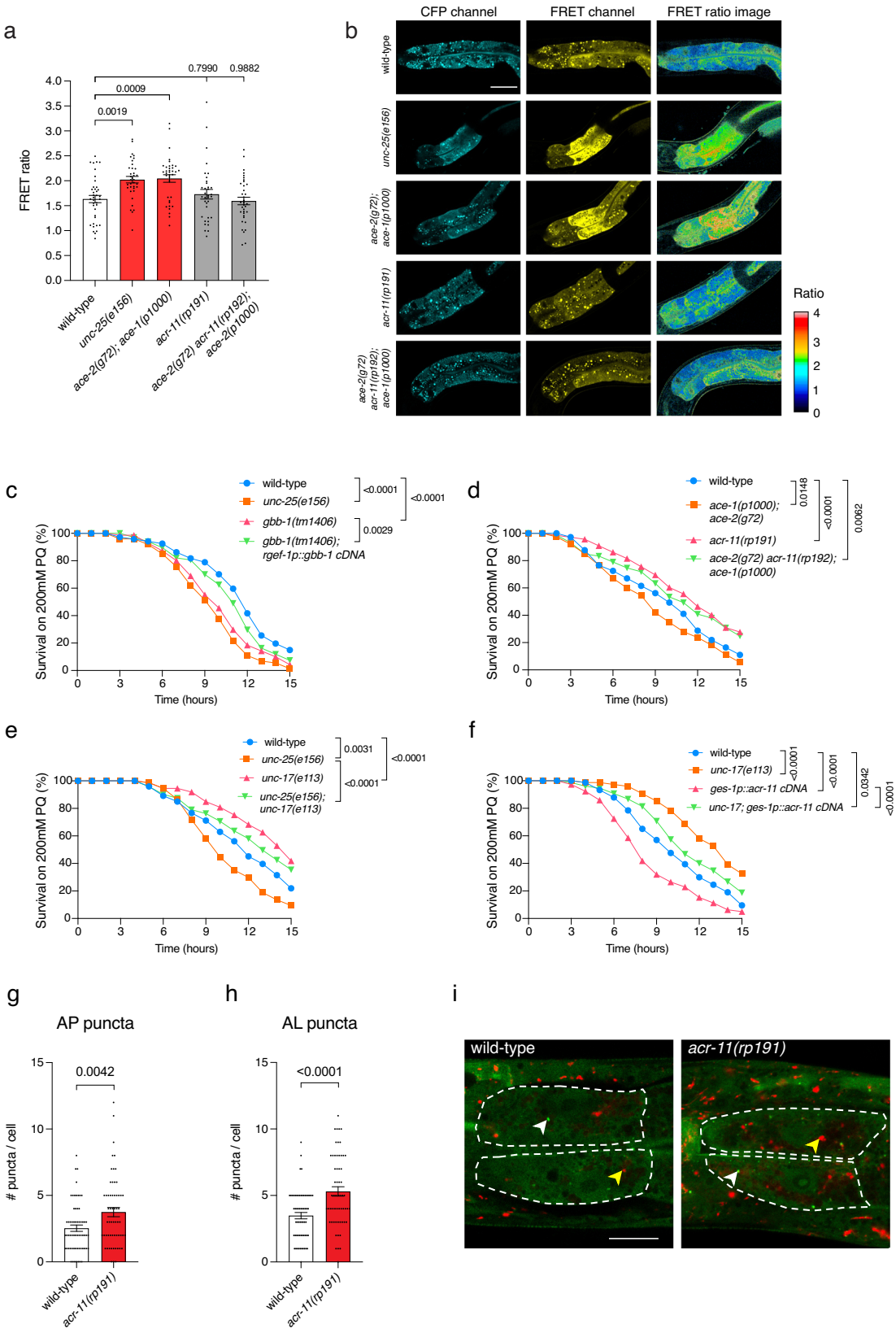

Stellaris5 Invert Confocal Microscope and objective lens 63×/1.40 Oil (WD 140 µm). CFP (405 excitation, 455–495 emission) and FRET (405 excitation, 515–555 emission) were collected. The FRET ratio in the first three intestinal cell pairs was calculated as (FRETint − FRETbg)/(CFPint − CFPbg).

Mitochondrial morphology analysis

Worms were anesthetised with 50 mM sodium azide diluted in M9 and mounted to 5% agarose pads. Images were taken using Leica Stellaris5 Invert Confocal Microscope and objective lens 63×/1.40 Oil (WD 140 µm). Optical slice thickness was 0.2 µm. Z stack images were

Fig. 5 | GABA/Ach regulation of ACR-11 influences mitochondrial stress resistance. a, **b** Quantification (**a**) and micrographs (**b**) of calcium imaging by FRET microscopy of the two anterior intestinal cells of wild-type, *unc-25(e156)*, *ace-2(g72); ace-1(p1000)*, *acr-11(rp191)* and *ace-2(g72) acr-11(rp192); ace-1(p1000)* animals expressing *nhx-2p::D3cpv*, a ratiometric indicator. $n = 38, 36, 36, 35, 36$ animals (left to right). Scale bar, 50 μm. Note that induced expression of the ratiometric reporter in animals with excess ACh (*unc-25* and *ace2; ace-1* mutants) in intestinal cells Int1-3 was consistent in all animals and not due to mosaicism. **c** Survival analysis of wild-type, *unc-25(e156)*, *gbb-1(tm1406)* and *gbb-1(tm1406); rgef-1p::gbb-1 cDNA* animals exposed to 200 mM paraquat from the L4 larval stage. $n = 67, 74, 70, 67$ animals (top to bottom). **d** Survival analysis of wild-type, *ace-2(g72); ace-1(p1000)*, *acr-11(rp191)* and *ace-2(g72) acr-11(rp192); ace-1(p1000)* animals exposed to 200 mM paraquat from the L4 larval stage. $n = 73, 72, 65, 67$ animals (top to bottom). **e** Survival analysis of wild-type, *unc-25(e156)*, *unc-17(e113)* and *unc-25(e156); unc-17(e113)* animals exposed to 200 mM paraquat from the L4 larval stage. $n = 73, 74, 72, 71$ animals (top to bottom). **f** Survival analysis of wild-type, *unc-17(e113)*, *ges-1p::acr-11 cDNA* and *unc-17(e113); ges-1p::acr-11 cDNA* animals exposed to 200 mM paraquat from the L4 larval stage. $n = 74, 74, 64, 75$ animals (top to bottom). **g**–**i** Quantification of (**g**) autophagosome puncta (AP), (**h**) autolysosome puncta (AL), and micrographs (**i**) of GFP and mCherry fluorescence in the two anterior intestinal cells of wild-type and *acr-11(rp191)* L4 larvae expressing LGG-1p::mCherry::GFP::LGG-1. White arrows = green puncta/autophagosomes, yellow arrows = red puncta/autolysosomes. $n = 62$ (wild type) and 59 *(acr-11(rp191)* animals). Scale bar, 5 μm. *P* values assessed by one-way analysis of variance (ANOVA) with Tukey's post hoc test (**a**), two-way analysis of variance (ANOVA) with Tukey's post hoc test (**c**–**f**), and two-way unpaired *t* test with Welch's correction (**g**, **h**). Error bars indicate SEM. Source data are provided as a Source Data file.

blinded to genotype and mitochondrial morphology classified as fused, intermediate or fragmented[6].

Acute paraquat sensitivity assays

200 mM paraquat plates were prepared[51] and seeded with 50 μl 10× concentrated OP50. 25 L4 worms were transferred to each plate and survival was assessed each hour for 15 consecutive hours. Worms that left the agar were excluded from analysis.

Autophagy analysis

Intestinal autophagy was analyzed using the *lgg-1p::mCherry::gfp::lgg-1* reporter[49]. A single image was taken in line with the nucleus of the first two intestinal cells using a Zeiss AXIO Imager M2 upright fluorescence microscope as described above. Images were blinded to genotype and green and red LGG-1 puncta were counted, with green puncta representing autophagosomes and red puncta representing autolysosomes.

Statistics and reproducibility

Statistical analysis was performed using GraphPad Prism 9 software. Statistical tests and *n* numbers are indicated in corresponding figure legends. Differences with a P value < 0.05 were considered significant. All experiments were performed with at least three independent biological replicates, with similar results; the investigator was blinded to the genotype. No statistical method was used to pre-determine sample size. No data were excluded from analysis. The experiments were not randomized.

Reporting summary

Further information on research design is available in the Nature Portfolio Reporting Summary linked to this article.

Data availability

All data is available in the main text or supplementary materials. There are no accession codes, unique identifiers, or weblinks in our study and no restrictions on data availability. Materials will be available upon request from the Pocock laboratory. Source data are provided with this paper.

References

1. Durieux, J., Wolff, S. & Dillin, A. The cell-non-autonomous nature of electron transport chain-mediated longevity. *Cell* **144**, 79–91 (2011).
2. Berendzen, K. M. et al. Neuroendocrine coordination of mitochondrial stress signaling and proteostasis. *Cell* **166**, 1553–1563.e1510 (2016).
3. Shao, L.-W., Niu, R. & Liu, Y. Neuropeptide signals cell non-autonomous mitochondrial unfolded protein response. *Cell Res.* **26**, 1182–1196 (2016).
4. Zhang, Q. et al. The mitochondrial unfolded protein response is mediated cell-non-autonomously by retromer-dependent Wnt signaling. *Cell* **174**, 870–883.e817 (2018).
5. Lan, J. et al. Translational regulation of non-autonomous mitochondrial stress response promotes longevity. *Cell Rep.* **28**, 1050–1062.e1056 (2019).
6. Zhang, Y. et al. Neuronal TORC1 modulates longevity via AMPK and cell nonautonomous regulation of mitochondrial dynamics in *C. elegans*. *eLife* **8**, e49158 (2019).
7. Chen, L. T. et al. Neuronal mitochondrial dynamics coordinate systemic mitochondrial morphology and stress response to confer pathogen resistance in C. elegans. *Dev. Cell* **56**, 1770–1785.e1712 (2021).
8. Yoneda, T. et al. Compartment-specific perturbation of protein handling activates genes encoding mitochondrial chaperones. *J. Cell Sci.* **117**, 4055–4066 (2004).
9. Andrew, M. & Cole, M. H. UPRmt regulation and output: a stress response mediated by mitochondrial-nuclear communication. *Cell Res.* **28**, 281–295 (2018).
10. Haynes, C. M., Petrova, K., Benedetti, C., Yang, Y. & Ron, D. ClpP mediates activation of a mitochondrial unfolded protein response in C. elegans. *Dev. Cell* **13**, 467–480 (2007).
11. Nargund, A. M., Pellegrino, M. W., Fiorese, C. J., Baker, B. M. & Haynes, C. M. Mitochondrial import efficiency of ATFS-1 regulates mitochondrial UPR activation. *Science* **337**, 587 (2012).
12. Nargund, A. M., Fiorese, C. J., Pellegrino, M. W., Deng, P. & Haynes, C. M. Mitochondrial and nuclear accumulation of the transcription factor ATFS-1 promotes OXPHOS recovery during the UPR(mt). *Mol. Cell* **58**, 123 (2015).
13. Omura, D. T., Clark, D. A., Samuel, A. D. & Horvitz, H. R. Dopamine signaling is essential for precise rates of locomotion by *C. elegans*. *PLoS ONE* **7**, e38649 (2012).
14. Alkema, M. J., Hunter-Ensor, M., Ringstad, N. & Horvitz, H. R. Tyramine functions independently of octopamine in the *Caenorhabditis elegans* nervous system. *Neuron* **46**, 247–260 (2005).
15. Sze, J. Y., Victor, M., Loer, C., Shi, Y. & Ruvkun, G. Food and metabolic signalling defects in a *Caenorhabditis elegans* serotonin-synthesis mutant. *Nature* **403**, 560–564 (2000).
16. Rankin, C. H. & Wicks, S. R. Mutations of the *Caenorhabditis elegans* brain-specific inorganic phosphate transporter eat-4 affect habituation of the tap-withdrawal response without affecting the response itself. *J. Neurosci.* **20**, 4337–4344 (2000).
17. Jin, Y., Jorgensen, E., Hartwieg, E. & Horvitz, H. R. The *Caenorhabditis elegans* gene unc-25 encodes glutamic acid decarboxylase and is required for synaptic transmission but not synaptic development. *J. Neurosci.* **19**, 539–548 (1999).

18. Rand, J. B. Genetic analysis of the cha-1-unc-17 gene complex in Caenorhabditis. *Genetics* **122**, 73–80 (1989).
19. Liu, J. et al. GABAergic signaling between enteric neurons and intestinal smooth muscle promotes innate immunity and gut defense in *Caenorhabditis elegans*. *Immunity* **56**, 1515–1532.e1519 (2023).
20. Chun, L. et al. Metabotropic GABA signalling modulates longevity in *C. elegans*. *Nat. Commun.* **6**, 8828 (2015).
21. Yuan, F. et al. GABA receptors differentially regulate life span and health span in *C. elegans* through distinct downstream mechanisms. *Am. J. Physiol.* **317**, C953–C963 (2019).
22. Haynes, C. M., Yang, Y., Blais, S. P., Neubert, T. A. & Ron, D. The matrix peptide exporter HAF-1 signals a mitochondrial UPR by activating the transcription factor ZC376.7 in *C. elegans*. *Mol. Cell* **37**, 529–540 (2010).
23. The *C. elegans* Deletion Mutant Consortium. Large-scale screening for targeted knockouts in the *Caenorhabditis elegans* genome. *G3 (Bethesda)* **2**, 1415–1425 (2012).
24. McIntire, S. L., Reimer, R. J., Schuske, K., Edwards, R. H. & Jorgensen, E. M. Identification and characterization of the vesicular GABA transporter. *Nature* **389**, 870–876 (1997).
25. Jin, Y., Hoskins, R. & Horvitz, H. R. Control of type-D GABAergic neuron differentiation by *C. elegans* UNC-30 homeodomain protein. *Nature* **372**, 780–783 (1994).
26. Eastman, C., Horvitz, H. R. & Jin, Y. Coordinated transcriptional regulation of the unc-25 glutamic acid decarboxylase and the unc-47 GABA vesicular transporter by the *Caenorhabditis elegans* UNC-30 homeodomain protein. *J. Neurosci.* **19**, 6225–6234 (1999).
27. Shore, D. E., Carr, C. E. & Ruvkun, G. Induction of cytoprotective pathways is central to the extension of lifespan conferred by multiple longevity pathways. *PLoS Genet.* **8**, e1002792 (2012).
28. Zhu, D. et al. NuRD mediates mitochondrial stress–induced longevity via chromatin remodeling in response to acetyl-CoA level. *Sci. Adv.* **6**, eabb2529 (2020).
29. Miller, K. G., Emerson, M. D. & Rand, J. B. Goalpha and diacylglycerol kinase negatively regulate the Gqalpha pathway in *C. elegans*. *Neuron* **24**, 323–333 (1999).
30. Yogeeswari, P., Sriram, D. & Vaigundaragavendran, J. The GABA shunt: an attractive and potential therapeutic target in the treatment of epileptic disorders. *Curr. Drug Metab.* **6**, 127–139 (2005).
31. Bamber, B. A., Beg, A. A., Twyman, R. E. & Jorgensen, E. M. The *Caenorhabditis elegans* unc-49 locus encodes multiple subunits of a heteromultimeric GABA receptor. *J. Neurosci.* **19**, 5348–5359 (1999).
32. Beg, A. A. & Jorgensen, E. M. EXP-1 is an excitatory GABA-gated cation channel. *Nat. Neurosci.* **6**, 1145–1152 (2003).
33. Taylor, S. R. et al. Molecular topography of an entire nervous system. *Cell* **184**, 4329–4347 e4323 (2021).
34. Cook, S. J. et al. Whole-animal connectomes of both *Caenorhabditis elegans* sexes. *Nature* **571**, 63–71 (2019).
35. Dittman, J. S. & Kaplan, J. M. Behavioral impact of neurotransmitter-activated G-protein-coupled receptors: muscarinic and GABAB receptors regulate *Caenorhabditis elegans* locomotion. *J. Neurosci.* **28**, 7104–7112 (2008).
36. Gao, S. et al. Excitatory motor neurons are local oscillators for backward locomotion. *Elife* **7**, e29915 (2018).
37. Schultheis, C., Brauner, M., Liewald, J. F. & Gottschalk, A. Optogenetic analysis of GABAB receptor signaling in *Caenorhabditis elegans* motor neurons. *J. Neurophysiol.* **106**, 817–827 (2011).
38. Lee, J., Kim, K. Y. & Paik, Y. K. Alteration in cellular acetylcholine influences dauer formation in *Caenorhabditis elegans*. *BMB Rep.* **47**, 80–85 (2014).
39. Glancy, B., Willis, W. T., Chess, D. J. & Balaban, R. S. Effect of calcium on the oxidative phosphorylation cascade in skeletal muscle mitochondria. *Biochemistry* **52**, 2793–2809 (2013).
40. Joiner, M.-lA. et al. CaMKII determines mitochondrial stress responses in heart. *Nature* **491**, 269–273 (2012).
41. Shen, J. X. & Yakel, J. L. Nicotinic acetylcholine receptor-mediated calcium signaling in the nervous system. *Acta Pharm. Sin.* **30**, 673–680 (2009).
42. Palmer, A. E. & Tsien, R. Y. Measuring calcium signaling using genetically targetable fluorescent indicators. *Nat. Protoc.* **1**, 1057–1065 (2006).
43. Zhang, F. et al. Bacillus thuringiensis crystal protein Cry6Aa triggers *Caenorhabditis elegans* necrosis pathway mediated by aspartic protease (ASP-1). *PLOS Pathog.* **12**, e1005389 (2016).
44. Sprenger, H. G. & Langer, T. The good and the bad of mitochondrial breakups. *Trends Cell Biol.* **29**, 888–900 (2019).
45. Cochemé, H. M. & Murphy, M. P. Complex I is the major site of mitochondrial superoxide production by paraquat. *J. Biol. Chem.* **283**, 1786–1798 (2008).
46. Adebayo, M., Singh, S., Singh, A. P. & Dasgupta, S. Mitochondrial fusion and fission: The fine-tune balance for cellular homeostasis. *FASEB J.* **35**, e21620 (2021).
47. Benedetti, C., Haynes, C. M., Yang, Y., Harding, H. P. & Ron, D. Ubiquitin-like protein 5 positively regulates chaperone gene expression in the mitochondrial unfolded protein response. (Author abstract). *Genetics* **174**, 229 (2006).
48. Raiders, S. A., Eastwood, M. D., Bacher, M. & Priess, J. R. Binucleate germ cells in *Caenorhabditis elegans* are removed by physiological apoptosis. *PLOS Genet.* **14**, e1007417 (2018).
49. Chang, J. T., Kumsta, C., Hellman, A. B., Adams, L. M. & Hansen, M. Spatiotemporal regulation of autophagy during *Caenorhabditis elegans* aging. *Elife* **6**, e18459 (2017).
50. Gergalova, G. et al. Mitochondria express alpha7 nicotinic acetylcholine receptors to regulate Ca2+ accumulation and cytochrome c release: study on isolated mitochondria. *PLoS ONE* **7**, e31361 (2012).
51. Senchuk, M. M., Dues, D. J. & Van Raamsdonk, J. M. Measuring oxidative stress in *Caenorhabditis elegans*: paraquat and juglone sensitivity assays. *Bio Protoc.* **7**, e2086 (2017).

Acknowledgements

We thank members of the Pocock laboratory for advice and comments on the paper. Imaging for this project was performed at Monash Microimaging. Some strains were provided by the *Caenorhabditis* Genetics Center (University of Minnesota), which is funded by the NIH Office of Research Infrastructure Programs (P40 OD010440) and National BioResource Project of Japan. We thank Shawn Xu, Haijun Tu and Jianfeng Liu for strains and plasmids. This work was supported by the following grants: National Health and Medical Research Council GNT1105374, GNT1137645, GNT2000766 and veski Innovation Fellowship (VIF23) to R.P.

Author contributions

Conceptualization: R.C., R.P. Methodology: R.C., W.C., A.H., B.H., R.G., R.P. Investigation: R.C., W.C., A.H., B.H., R.G., R.P. Visualization: R.C., W.C., A.H., B.H. Funding acquisition: R.P. Project administration: R.P. Supervision: A.H., R.P. Writing—original draft: R.C. Writing—review & editing: W.C., A.H., B.H., R.G., R.P.

Competing interests

The authors declare no competing interests.

Additional information

Supplementary information The online version contains supplementary material available at https://doi.org/10.1038/s41467-024-50973-y.

Correspondence and requests for materials should be addressed to Roger Pocock.

Peer review information *Nature Communications* thanks the anonymous reviewer(s) for their contribution to the peer review of this work. A peer review file is available.